Characterization of aberrant splicing in pediatric central nervous system tumors reveals *CLK1* as a candidate oncogenic dependency

Ammar S. Naqvi[1,2,+], Patricia J. Sullivan[3,+], Ryan J. Corbett[3], Priyanka Sehgal[4], Karina L. Conkrite[5], Komal S. Rathi[1,2], Brian M. Ennis[1,2], Katharina E Hayer[6], Bo Zhang[1,2], Miguel A. Brown[1,2], Daniel P. Miller[1,2], Alex Sickler[3], Adam A. Kraya[1,2], Kaleem L. Coleman[3], Joseph M. Dybas[1,2], Zhuangzhuang Geng[1,2], Christopher Blackden[1,2], Shehbeel Arif[1,2], Antonia Chroni[1,2], Aditya Lahiri[6], Madison L. Hollawell[1,2], Phillip B. Storm[1,2], Dalia Haydar[3,7], Jessica B. Foster[5,8], Mateusz Koptyra[1,2], Peter J. Madsen[1,2], Sharon J. Diskin[5,6,8], Andrei Thomas-Tikhonenko[4,5,8,9], Adam C. Resnick[1,2], Jo Lynne Rokita[3,7,*]

[1] Center for Data-Driven Discovery in Biomedicine, Children's Hospital of Philadelphia, Philadelphia, PA, USA

[2] Division of Neurosurgery, Children's Hospital of Philadelphia, Philadelphia, PA, USA

[3] Center for Cancer and Immunology Research, Children's National Hospital, Washington, D.C., USA

[4] Division of Cancer Pathobiology, Children's Hospital of Philadelphia, Philadelphia, PA, USA

[5] Division of Oncology and Center for Childhood Cancer Research, Children's Hospital of Philadelphia, Philadelphia, PA

[6] Department of Biomedical and Health Informatics, Children's Hospital of Philadelphia, Philadelphia, PA, USA

[7] Department of Pediatrics, The George Washington University School of Medicine and Health Sciences, Washington, D.C., USA

[8] Department of Pediatrics, University of Pennsylvania, Philadelphia, PA, USA

[9] Department of Pathology and Laboratory Medicine, University of Pennsylvania, Philadelphia, PA, USA

[+]Authors contributed equally

*Correspondence:

Jo Lynne Rokita, Ph.D.

Children's National Hospital

Abstract

Background: Pediatric brain cancer is the leading cause of disease-related mortality in children, yet many aggressive tumors lack effective therapies. Aberrant RNA splicing is a hallmark of cancer, but its role in pediatric central nervous system (CNS) tumors remains underexplored.

Methods: We analyzed 752 primary pediatric brain tumors spanning histologies and molecular subtypes to characterize aberrant splicing. We developed the *Splicing Burden Index (SBI)* as a sample-level metric and performed hierarchical clustering of variable splice events. Cluster-specific events were annotated for overlap with functional protein domains. We conducted *in vitro* experiments to assess the role of the splicing regulator *CDC-like kinase 1 (CLK1)*.

Results: Clustering identified 11 splicing-defined groups, several enriched for distinct tumor types, though heterogeneity was observed across histologies. Cluster 6, with the poorest event-free survival, comprised multiple histologies and contained 39,528 aberrant splice events across 10,412 genes, including 8,369 single exon (SE) events overlapping known functional protein domains. *CLK1* expression was most positively correlated with SE SBI in Cluster 6, and inclusion of its exon 4 (active kinase isoform) was widespread and associated with inferior event-free survival. Pharmacologic inhibition of *CLK1* with cirtuvivint suppressed viability and proliferation in KNS-42 cells, while morpholinos targeting exon 4 reduced *CLK1* RNA and protein abundance, impaired growth, and induced splicing and expression changes in cancer-related genes.

Conclusions: This study maps splicing dysregulation in pediatric brain tumors, defines biologically- and clinically-relevant splicing-defined subgroups, and identifies *CLK1* as a

regulator of oncogenic splicing programs. These findings support therapeutic targeting of splicing kinases in high-risk pediatric CNS tumors.

Keywords: aberrant splicing, pediatric brain tumors, *CLK1*, oncogenic dependency, therapeutic targeting

Key Points

- Splicing profiles of 752 pediatric CNS tumors define 11 clusters linked to histology
- *CLK1* exon 4 inclusion is widespread in CNS tumors, producing active kinase isoform
- High *CLK1* exon 4 inclusion predicts poor prognosis in aggressive CNS tumors

Importance of study

This study systematically characterizes alternative splicing across 752 primary pediatric central nervous system (CNS) tumors and reveals extensive heterogeneity in splicing programs. We identify 11 distinct splicing-defined clusters, with *Cluster 6* enriched for aberrant splice events, transcriptional dysregulation, and poor clinical outcomes. Within this high-burden cluster, *CDC-like kinase 1 (CLK1)* exon 4 was differentially spliced with higher inclusion significantly associated with worse event-free survival. Functional experiments show that pharmacological inhibition or splice-modulating depletion of *CLK1* significantly reduces tumor cell viability and proliferation, while altering the expression and splicing of numerous cancer-associated genes. These findings underscore the fundamental role of RNA splicing in the biology of pediatric brain tumors, the relevance of splice-defined tumor subgroups, and highlight splicing modulation as a promising therapeutic strategy in pediatric CNS tumors.

Introduction

Pediatric brain cancer is the number one cause of disease-related death in children[1]. Furthermore, pediatric high-grade gliomas (HGGs) are largely resistant to chemotherapy and are often surgically unresectable, making them exceptionally challenging[2]. Despite decades of clinical trials in pediatrics, patients with certain tumor types such as diffuse intrinsic pontine glioma (DIPG) or diffuse midline glioma (DMG) will succumb to their disease, with a median overall survival of 11 months in patients[3]. Even with optimal multimodal therapy, median overall survival for non-DMG patients with a HGG is 14-20 months[4].

Within the last decade, advances in surgical biopsy, autopsy donation, and sequencing have enabled genomic characterization of pediatric HGGs, revealing recurrent somatic drivers including mutations, fusions, and copy number alterations. However, the role of alternative splicing, a key post-transcriptional regulatory mechanism, remains underexplored in these tumors. Previous studies have identified rare, mutually exclusive mutations in spliceosome-associated factors such as *SF3B1* and *SF3B2* in pediatric HGGs, which disrupt cellular processes involved in maintenance of DNA replication, genome integrity, or transcriptional fidelity[5,6]. More recently, Siddaway, et. al. describe alternative aberrant splicing as a mechanism of oncogenic pathway activation in pediatric HGGs, including those in the RAS/MAPK pathway, leading to worse patient survival[7]. Furthermore, an alternatively spliced neuronal cell adhesion molecule (NRCAM) but not its canonical isoform was found to be essential for pHGG cell line-derived xenograft growth *in vivo*[8].

Alternative splicing plays essential roles in gene regulation, expanding proteomic diversity, modulating transcript stability, and controlling protein localization, folding, and function[9,10]. The mammalian brain exhibits the most complex and conserved alternative splicing programs of any tissue, and their disruption is associated with a variety of neurodevelopmental disorders and neurological diseases[11,12]. Splicing regulation is tightly governed by *trans*-acting RNA-binding proteins (RBPs), such as the Serine-rich Splicing Factors (SRSFs), which bind to

regulatory sequences on preliminary mRNA transcripts. Disturbing that balance or their regulators can be detrimental to cellular functionality and result in oncogenic transformation[13,14].

To date, however, comprehensive analysis of alternative splicing across pediatric CNS tumors has not been performed. While prior work has focused on HGGs, the broader role across diverse pediatric brain tumor types remains unknown. In this study, we perform a large-scale analysis of genome-wide alternative splicing across 752 pediatric CNS tumors encompassing a wide range of histologic and molecular subtypes. We uncover widespread splicing alterations that reveal unique splicing biology within and across histologies and/or molecular subtypes. Many of these events are predicted to disrupt known protein domains, potentially altering function. We identify and experimentally characterize *CLK1* as a candidate oncogenic dependency in pediatric CNS tumors and propose that targeting aberrant splicing and/or its resulting downstream proteins may offer additional therapeutic avenues for precision cancer therapy.

Materials and Methods

Study participants and patient-derived cell line models

Study participants include pediatric brain tumor patients whose genomic data were deposited into and obtained from the OpenPedCan[15] project. Histologies include Atypical Teratoid Rhabdoid Tumor (ATRT, N = 56), choroid plexus tumor (CPT, N = 32), craniopharyngioma (CPG, N = 51), diffuse intrinsic pontine glioma or diffuse midline glioma (DIPG or DMG, N = 135), ependymoma (N = 110), germ cell tumor (N = 16), low-grade glioma (LGG, N = 337), medulloblastoma (MB, N = 200), meningioma (N = 29), mesenchymal tumor (N = 26), mixed neuronal-glial tumor (GNT, N = 112), neurofibroma plexiform (N = 12), non-neoplastic tumor (N = 45), other CNS embryonic tumor (N = 16), other high-grade glioma (other HGG, N = 190), schwannoma (N = 21), and other rare brain tumors (N = 27).

Primary data analyses

Somatic primary workflows were implemented by the Kids First Data Resource Center as described in the Open Pediatric Brain Tumor Atlas (OpenPBTA)[16] and OpenPedCan[15] projects. The code for these workflows, including RNA-seq quantification, fusion identification, RNA splicing, and SNV, INDEL, CNV, SV calling, can be found at https://github.com/d3b-center/OpenPedCan-workflows. Sample-level data can be found through the Kids First Portal at https://kidsfirstdrc.org/. To detect alternative splicing, we ran rMATS turbo (v. 4.1.0)[17] with GENCODE v39 GFF annotations on single samples, as described by the Kids First RNA-Seq workflow (https://github.com/d3b-center/OpenPedCan-workflows). We filtered for alternative splicing events with ≥ 10 junction read counts. To compare RNA-Seq from *CLK1* exon 4 morpholino-treated cells vs control morpholino-treated cells, we ran rMATs with three biological replicates for each condition `--b1 –b2`. This paired mode analysis calculated ΔPSI, p-values, and FDR statistics for each splice event. These results were then used for all downstream processing throughout the manuscript.

Cell Culture

The high-grade glioma patient-derived cell lines 7316-1763 and 7316-1769 were obtained by CBTN request, and the KNS-42 cell line was obtained from Accegen (ABC-TC0532). The pediatric HGG cell line KNS-42 was cultured in DMEM-F12 (GIBCO, 11320033) supplemented with 10% FBS (GIBCO, 26140079), 2 mmol/L L-glutamine (GIBCO, 25030081), and 1X penicillin/streptomycin (GIBCO, 15140122) at 37°C and 5% CO_2. The cell line was authenticated by Guardian Forensic Sciences (Abington, PA) using the GenePrint 24 (Promega, B1870) short tandem repeat kit. Cells tested negative for mycoplasma using the EZ-PCR

Mycoplasma Detection Kit (Biological Industries, 20-700-20) and were used for a maximum of 12 passages post thaw.

Morpholino Treatments

A Vivo-Morpholino ACTCTTCTGGAAACGTCAAGTGGGC (Gene Tools, LLC) targeting the intron 3-exon 4 splice junction was used to skip exon 4 in *CLK1*. Cells were treated with 1, 5, and 10 μM concentrations of *CLK1* morpholino and 10 μM of Control morpholino. 48 hours post-treatment, cells were harvested for PCR and immunoblots.

RNA Extraction and Quantitative Real-time PCR (qRT-PCR)

Total RNA was isolated and treated with DNAse using the Maxwell RSC simplyRNA Cells kit (Promega, AS1390) with the Maxwell RSC48 Instrument (Promega) per the manufacturer's instructions. Next, 2 μg of RNA were reverse-transcribed using SuperScript IV (Invitrogen, 18090010). Primers used for *CLK1* mRNA transcript quantification are listed in **TableS6J**. qRT-PCR was performed using PowerSYBR Green PCR Master Mix (Invitrogen, 4367659) on an Applied Biosystems Viia7 machine. The amplification was performed using the following settings: denaturation at 95°C for 10 min, followed by 40 cycles of denaturation at 95°C for 15 s and annealing at 60°C for 1 min. The comparative cycle threshold (CT) method was applied to quantify the expression levels of *CLK1*. The fold change of gene expression was calculated by the equation 2ΔΔCT, with *HPRT* (Thermo Fisher, 4453320, assay ID: Hs02800695_m1) used as the housekeeping gene.

Protein Extraction

Cultured cells were washed once in chilled D-PBS (pH 7.4) and lysed in RIPA buffer containing 50 mM Tris□HCl, pH 7.4, NP□40 (1%), deoxycholate (0.25%), 150 mM NaCl, 1 mM EDTA pH 8.0, 1x protease and phosphatase inhibitor cocktail (Pierce Halt Inhibitor Cocktail,

Thermo Fisher Scientific, 78446), and SDS (0.1%). Total protein in the lysate was estimated by the DC Protein assay (BioRad Laboratories, 5000111).

Detection of Proteins Using Immunoblot Analysis

70 µg of total protein were mixed with 5X SDS loading dye (Biorad, 161-0374) and resolved on 10% SDS polyacrylamide gel. The protein was transferred onto a PVDF membrane (Immobilin-P, Millipore, IPVH00010) and probed with α-CLK1 mouse monoclonal primary antibody (Santa Cruz, sc-515897) and HRP conjugated secondary antibody (Cell Signaling Technology, 7076S). Bands were detected using enhanced chemiluminescence (Millipore, WBKLS0500) and captured by a Chemiluminescence imager (GE Healthcare). β-actin was used as the loading control and probed with α-β-actin rabbit monoclonal antibody (Cell Signaling Technology, 12262S).

pan-DYRK/CLK1 inhibitor Cirtuvivint (SM08502) experiments

The KNS-42 cell line was cultured in DMEM-F12 (Gibco, 11330032) supplemented with 10% FBS (Corning, MT3501CV, lot 003322001) and additional L-glutamine (Thermo Fisher, 25030081) to a final concentration of 4.5 mM. Dissociation was performed with Trypsin-EDTA (0.05%, Thermo 25300054) and counted on a DeNovix Cell Drop cell counter.

For growth kinetics, 10,000 (3 day assay) or 6,000 (6 day assay) cells were plated per well into a 96-well plate (Greiner Bio-One, 655098) in a 200 uL total volume per well. Plates were placed into an Incucyte SX5 device and scanned every 2 hours for several days to measure growth via a mask designed uniquely for this cell type. At the end point of the assay, cell viability was analyzed with CellTiter Glo 2.0 reagent (Promega, G9242) by replacing half the media with reagent and reading on a Promega GloMax device.

Cirtuvivint (MedChem Express, HY-137435) was resuspended in 100% DMSO (Sigma, D2650-5X5ML) to 1 mM and stored in aliquots at -80 C. Dosing was optimized via serial dilution at a

range of 20 uM to 0.02 uM against a vehicle control equivalent to the highest dosing of drug. Cells were plated and at 24 hours, 100 uL of media were removed from each well and replaced with drug media for a final dose range of 0.01, 0.05, 0.5, 0.1, 1, 5, and 10 uM. Cells were untouched for 3 days total while growth was monitored via Incucyte.

Cell Viability Assay

Cell viability was measured using the CellTitre-Glo (CTG) luminescent cell viability assay (Promega, G7570). Cells were seeded in white 96-well flat-bottom plates at a density of 24,000 cells per well and treated the following day with either 7.5 μM control or CLK1 exon 4 targeted morpholino. Luminescence was measured using a Biotek Synergy 2 plate reader at 24, 48, 72, and 96 hours.

Results

Pediatric brain tumors display heterogeneous global patterns of aberrant splicing

To investigate alternative splicing in pediatric brain tumors, we analyzed stranded total RNA-Seq data for 752 diagnostic tumors from the Open Pediatric Cancer (OpenPedCan) project[15] (**Figure 1A**). Demographic and clinical data for each patient and tumor in this study are available in **Table S1**. We quantified splicing events at single-sample resolution using percent-spliced-in (PSI) values derived from replicate Multivariate Analysis of Transcript splicing (rMATS)[17,18] to identify skipped exon (SE), alternative 5' splice site (A5SS), alternative 3' splice site (A3SS), and retained intron (RI) events.

Due to the diverse biological and molecular drivers of these CNS cancers, we hypothesized that we might observe distinct splicing patterns across histologies and/or molecular subtypes. Among recurrent (N ≥ 2) differential splice events, SE events were the

most frequently observed (**Figure 1B**), consistent with a previous report in pediatric HGGs[7]. We then explored whether these SE events were histology-specific or shared events across tumor types. Indeed, we observed both shared and histology-specific SE events (**Figure 1C**), with medulloblastoma (MB), low-grade glioma (LGG), and non-DIPG/DMG high-grade glioma (other HGG) tumors exhibiting the highest number of unique recurrent SE events. This pattern remained consistent after normalizing by the number of patients within each histology (**Figure 1D**). A complete list of unique events per histology is reported in **Table S2A**.

To enable cross-sample comparisons of alternative splicing, we devised the splicing burden index (SBI): a metric that quantifies the proportion of differential alternative splicing (AS) events in a sample (**Online Methods**). SBI is calculated using a single event type, with the following analysis focused on SE events. Across the cohort, the median SBI was 0.0356 (3.56%). Among tumor types, LGGs had the lowest median SBI at 2.05%, while germ cell tumors (GCTs) had the highest at 9.43% (**Figure 1E)**. SBI also revealed variability within tumor histologies. Tumors with high SBI variance (> 3rd quartile variance) indicate more heterogeneous tumors, including neurofibroma plexiform, other HGGs, GCTs, and other rare tumors. We performed a similar analysis using other splice types (Alternative 5' Splice Site [A5SS], Alternative 5' Splice Site [A3SS], and Retained Intron [RI]) and observed that LGGs continued to exhibit the lowest median SBI, while other rare tumors and GCTs maintained the highest median SBI (**Figures S1A-C**). Despite a relatively low splicing burden across all histologies, the observed variability highlights the nuanced tumor-specific and intra-tumoral heterogeneity of splicing programs in these CNS tumors.

We hypothesized that tumors with a low tumor mutation burden (TMB) might have a higher splicing burden index as an alternate mechanism driving tumorigenesis. However, we observed the opposite: a weak but significant positive correlation between TMB and SBI (Pearson's R = 0.15, p-value = 8.2e-5; **Figure S1D**), which persisted after excluding hyper-mutant tumors (R = 0.15, p-value = 7.4e-5, **Figure S1E**).

Splice events cluster pediatric brain tumor histologies and are associated with survival outcomes

To assess whether CNS tumors exhibit shared splicing patterns, we performed hierarchical clustering of samples using PSI values from the top 5,000 most variable SE events across all primary tumors (N = 752). This analysis revealed 11 distinct clusters, each enriched for specific histologies and/or molecular subtypes (**Figure 2A** and **S2A-E**). For instance, Clusters 10 and 11 were enriched for MB, with Cluster 10 showing significant enrichment for Group 4 (OR = 80.5, $p < 0.05$) and Cluster 11 enriched for the SHH subtype (OR = 5.1, $p < 0.05$) (**Figure S2B)**. These findings are consistent with prior work demonstrating that the MB subgroups WNT, SHH, Group 3, and Group 4 can be delineated based on splicing patterns[19]. Clusters 5 and 6 were significantly enriched for ATRT-MYC and ATRT-SHH subtypes, respectively (OR = 38.4 and 19.2, $p < 0.05$) (**Figure S2C**). HGGs, including DIPG/DMGs, exhibited the greatest splicing heterogeneity, with samples spanning 7 of the 11 identified clusters (**Figure S2D-E**). We examined event-free survival (EFS) across splicing-defined clusters and found that Cluster 6 was associated with the poorest EFS ($p < 0.001$) (**Figure 2B**). This cluster was predominantly comprised of HGGs, representing 75% of the group (**Figure 2C)**, along with a mix of additional histologies. Clusters 4, 8, and 9 demonstrated the most favorable EFS ($p < 0.05$); Cluster 4 was significantly enriched for non-neoplastic tumors, other HGGs (including H3 wildtype and H3 G35 tumors), and mixed neuronal-glial tumors (GNT); Cluster 8 for non-neoplastic tumors and GNTs; and Cluster 9 for neurofibromatosis-associated (NF) tumors (**Figure S2A**). A full list of samples with associated cluster membership information is outlined in **Table S2B**.

To explore the functional impact of splicing alterations, we identified differentially expressed cancer-associated signaling pathways in each of the 11 clusters (**Figure 2D)**. Strikingly, the spliceosome pathway was significantly upregulated in Cluster 6, the cluster with

the worst EFS (**Table S2C**, Log_2FC = 0.41, Bonf-adj p = 4.89e-13 vs. all other groups) and significantly downregulated in Clusters 4, 8, and 9, with significantly better EFS (**Table S2,** Bonf-adj p < 0.05). In addition, the epithelial mesenchymal transition (EMT) pathway was the most significantly differentially-expressed in Cluster 9 (**Table S2**, Bonf-adj p = 3.39e-9), enriched for NF tumors and consistent with a previous report demonstrating activated EMT in samples with NF-1 loss[20]. These results demonstrate that spliced genes can cluster into biologically meaningful groups, highlighting distinct pathways and gene targets within each cluster.

To evaluate whether upregulation of the KEGG spliceosome GSVA score translates into elevated protein expression, we investigated splicing factor protein levels by integrating gene expression and matched proteogenomic (N = 122) data from the Clinical Proteomic Tumor Analysis Consortium (CPTAC)[21]. We visualized protein (**Figure 2E**) and RNA (**Figure S2F**) expression of KEGG spliceosome pathway genes (**Table S3A**) alongside their corresponding GSVA scores and observed a significant positive correlation between protein abundance and KEGG spliceosome scores (R = 0.4, p = 2.6e-6; **Figure S2G**), suggesting that RNA expression can serve as a reliable readout for pathway activity.

We next assessed whether spliceosome activity, measured by GSVA score, was associated with survival outcomes across the cohort using a multivariate cox proportional hazards model adjusting for tumor resection, glioma grade group, age at diagnosis, and cluster. Favorable prognostic variables included tumor resection (HR = 0.31, p < 0.01) and Cluster 4 membership (HR = 0.26, p = 0.03), whereas non-LGG tumors (HR = 2.08, p < 0.01) and Cluster 6 membership (HR = 3.78, p < 0.01) were associated with worse EFS. Notably, we detected a significant interaction between spliceosome GSVA scores and Cluster 6, where higher spliceosome activity conferred a survival benefit (HR = 0.24, p = 0.04, **Figure 2F**). Given the prognostic effects of both spliceosome GSVA scores and SE SBI, we further tested their relationship using an interaction model, which revealed a significant synergistic effect (HR = 0.25, p < 0.01; **Figure S2H**). Together, these results suggest that elevated spliceosome activity,

particularly in tumors with high SE burden, may partially offset the poor prognosis associated with aggressive subgroups such as Cluster 6.

Widespread splicing alterations driven by expression changes in splicing factors

Since Cluster 6 exhibited marked upregulation of spliceosome pathways and the poorest event-free survival, we selected it for further investigation. This cluster also showed the greatest variability in SBI scores, with the largest interquartile range and overall spread across all clusters (**Figure S3A**), suggesting that splicing burden may influence outcomes within this aggressive group. Consistent with the protective effect of higher GSVA scores observed in **Figure 2F**, a multivariate model stratifying GSVA scores by quartile confirmed that tumors in the highest (4th) quartile had significantly better EFS than those in the lowest (1st) quartile (HR = 0.18, p = 0.03; **Figure S3B**). Similarly, in a separate model, higher SE SBI scores were significantly associated with improved overall survival in Cluster 6 (HR = 0.12, $p < 0.01$, **Figure 3A**), a finding further supported by Kaplan–Meier analysis showing significantly better overall survival for tumors in the highest versus lowest SBI quartile tumors (p = 0.041; **Figure S3C**).

To investigate the mechanisms driving the widespread splicing alterations, we first assessed somatic alterations in Cluster 6. Consistent with the high proportion of HGGs present in Cluster 6, we observed frequent mutations in *TP53* (55%), *H3-3A* (49%), and *ATRX* (42%) (**Figure S3D)**. Mutations in either HUGO spliceosome genes (**Table S2B**) or known splicing factor genes (**Table S2C**) were absent in Cluster 6 tumors and rare in the cohort overall (**Tables S3D-E)**, suggesting alternative regulatory mechanisms as drivers of the splicing alterations that define Cluster 6. It has been previously shown that in the absence of splicing factor gene mutations, RNA expression changes in these genes can cause downstream splicing changes to promote tumor formation[22–24]. Thus, we performed differential gene expression (DE) analysis between high vs low SBI tumors in Cluster 6 for known splicing factors and related genes[25] (**Table S3C**) and found 41.3% (N = 558/1350) to be significantly differentially expressed

(adjusted p-value < 0.05, **Figure 3B, Table S3F**). Specifically, 71.4% (20/28) genes encoding the serine/arginine-rich splicing factor (SRSF) and heterogeneous nuclear ribonucleoproteins (hnRNP) families of trans-acting splicing factors known to directly influence exon-associated splicing[26] were significantly DE between high vs low SBI tumors.

Recurrent splicing aberrations alter the inclusion of known functional sites in transcripts

To further elucidate the aberrant splicing landscape of Cluster 6, we developed a robust and adaptable workflow to prioritize recurrent (N ≥ 2) differentially spliced (ΔPSI z-score > |2|) SE events with predicted functional impact (**Figure 3C**). We identified 23,674 recurrent differential SE splicing events in Cluster 6 tumors. Of these, we prioritized 8,369 with a putative functional effect, defined by the gain or loss of a known Uniprot functional site. These functional sites included changes to disulfide bonding (N = 630), localization signaling (N = 284), amino acid modification (N = 1,533), and domains (N = 6,946) (**Table S4)**. To identify potentially targetable events, we selected functional splice events in kinases, resulting in 349 SE events. We reduced our focus to kinases with a known role in splicing regulation, narrowing our list of candidates to 14 SE events in 8 genes.

CDC-like kinase 1 (CLK1), a known master modulator of alternative splicing[13], was the most significantly correlated splicing factor related gene with Cluster 6 SE SBI (**Table S5, Figure 3E**). *CLK1* regulates the SR (Serine aRginine) family of splicing factor proteins through hyper-phosphorylation of the SR-rich peptide regions of SR proteins to induce cooperative RNA binding and increased activity[27–29]. Canonical *CLK1* requires exon 4 for activation[30]. We observed differential splicing of this exon, with seven tumors in Cluster 6 showing significant skipping (reduced inclusion) and an average ΔPSI of 0.437 (**Table S4D)**. We used a sashimi plot to illustrate this, contrasting tumors with high versus low exon inclusion (**Figure 3D**). The majority of tumors showed high levels of *CLK1* exon 4 inclusion (**Figure S3E**) with a mean PSI

of 0.790 and Cluster 6 showed the highest degree of variability of *CLK1* exon 4 PSI (**Figure S3F**).

Given the identification of *CLK1* exon 4 skipping as a recurrent event in Cluster 6 tumors, we examined whether *CLK1* expression was associated with overall splicing dysregulation. *CLK1* expression was significantly positively correlated with SE SBI in multiple clusters (**Figure S4A**), with the strongest correlation observed in Cluster 6 (Pearson's R = 0.70, p = 2e-11, FDR = 2.4e-8; **Figure 3E**). Notably, among all splicing factors and RNA binding proteins (N = 1,350)[25], *CLK1* expression showed the most significant positive correlation with SE SBI in Cluster 6. This relationship appeared to be driven by histology, with strong correlations observed in other HGGs (R = 0.67, p = 1.2e-13; **Figure S4B**) and DIPG/DMG tumors (R = 0.52, p = 0.0021; **Figure S4B**). Furthermore, expression of the canonical transcript ENST00000321356, which includes exon 4, was positively correlated with exon 4 PSI in Cluster 6 (R = 0.62, p = 3.8e-08; **Figure 3E**), as well as in all other clusters except Cluster 9 (**Figure S4C)**. In Cluster 6, tumors with high *CLK1* exon 4 PSI had significantly worse OS (HR = 18.98, p = 0.03, **Figure 3F**) and EFS (HR = 78.63, p = 0.01, **Figure 3G**), even accounting for clinical covariates, suggesting a *CLK1*-associated splicing state rather than generalized spliceosome activation. Finally, we assessed *CLK1* exon 4 inclusion in non-tumor brain tissues using RNA-Seq data from the Evolutionary Developmental (Evo-Devo) Atlas (N = 59)[31] and GTEx (N=2,642). *CLK1* exon 4 inclusion was significantly higher in Cluster 6 compared to GTEx but comparable to fetal Evo-Devo samples, and decreased with age across non-tumor tissues ($p < 0.05$), consistent with an oncofetal splicing pattern (**Figure 3H**). Together, these findings highlight *CLK1* exon 4 inclusion as a recurrent, functionally relevant splicing aberration in Cluster 6 tumors linked to widespread splicing dysregulation, adverse clinical outcomes, and an oncofetal splicing pattern, underscoring its potential as a biologically meaningful and therapeutically relevant target.

***CLK1* is an oncogenic dependency in pediatric CNS tumors**

To experimentally test our findings from Cluster 6 tumors, we sought to evaluate *CLK1* and exon 4 inclusion as potential dependencies and therapeutic targets in pediatric brain tumor cell lines. We investigated the cancer Dependency Map (DepMap) portal and database and found that CNS and brain tumor cell lines with high expression of the exon 4 included transcript of *CLK1* (≥ third quantile mRNA expression of ENST00000321356) have significantly higher CRISPR dependency (lower scores) compared to *CLK1* low expressing cell lines (≤ first quantile) (Wilcoxon $p = 0.034$, **Figure 4A**). This observation was significant only to cell lines derived from CNS tumor and myeloid malignancies (**Figure S5A**), suggesting tissue- and tumor-specific regulation of *CLK1*. Of the DepMap profiled cell lines, the pediatric glioblastoma cell line KNS-42 had a strong dependency on *CLK1* (**Figure 4B**) and hence was chosen for further *in vitro* testing, along with two additional cell lines from our pediatric brain tumor cohort with high *CLK1* exon 4 PSI (7316-1763 and 7316-1769). We experimentally validated the exon 4 splice event identified from short-read RNA-Seq. Specifically, we performed long-read RNA-seq using Oxford Nanopore Technologies (ONT), which confirmed that these patient-derived cell lines contain a similar ratio of *CLK1* mRNA isoforms that either include or skip exon 4 (**Figure 4C**).

Next, we tested the impact of CLK1 inhibition in KNS-42 cells using the pan-Dyrk/Clk inhibitor cirtuvivint (SM08502)[32]. Using the IncuCyte Live Cell Analysis System to monitor real-time proliferation, we observed a significant reduction in cell growth at multiple concentrations over a 6-day period (**Figure 4D**). Additionally, we observed a dose-dependent decrease in cell viability using CellTiter-Glo at three days (**Figure 4E**) and six days (**Figure S5B**) post-treatment of 0.5, 1, 5, and 10 μM Cirtuvivint.

CLK1 regulates the SR (Serine aRginine) family of splicing factor proteins through hyper-phosphorylation of the SR-rich peptide regions of SR proteins to induce cooperative RNA

binding and increased activity[27–29]. We therefore postulated that the gain of *CLK1* exon 4 increases mRNA and subsequent protein production. To directly test this hypothesis, we modulated *CLK1* exon 4 splicing using targeted morpholino oligomers (see **Online Methods**), in which we forced exon 4 skipping in the KNS-42 cell line. We performed qRT-PCR and observed a near total loss of the *CLK1* exon 4 inclusion transcript at both 5 and 10 μM of exon 4 targeted morpholino, evidenced by reduced expression of the exon 3-4 junction. At these same concentrations, we observed increased *CLK1* exon 4 skipping using primers targeting the exon 3-5 junction (**Figure 4F**). Importantly, forced *CLK1* exon 4 skipping resulted in ablation of CLK1 protein at 5 and 10 μM (**Figure 4G),** corroborating previous work that *CLK1* exon 4 is required for full-length and catalytically active *CLK1*[33–35]. Next, we assessed the functional impact of *CLK1* exon 4 splicing using CellTiter-Glo and confirmed that cells with high *CLK1* exon 4 skipping (*CLK1* exon 4 targeting morpholino) exhibited significantly decreased viability compared to those with *CLK1* exon 4 inclusion (non-targeting morpholino) at 24, 72, and 96 hours ($p \leq 0.01$, within-time Student's *t-test*, **Figure 4H**). Taken together, we demonstrate that *CLK1* is a dependency in pediatric CNS tumors, required for cellular growth and viability in pediatric HGGs, and *CLK1* mRNA and protein is maintained through increased exon 4 inclusion.

To identify *CLK1* targets mediated by exon 4 splicing, we performed RNA-seq from KNS-42 cells treated with morpholino oligomers (N = 3 controls, N = 3 targeted to skip exon 4). We performed differential gene expression (DE) analysis and identified 1,322 genes with differential expression (569 upregulated, 753 downregulated) between cells treated with morpholino or non-targeting control (**Figure 5A, Table S6A**), including 79 oncogenes or tumor suppressor genes (TSGs, **Figure 5B**). Next, we identified a total of 8,741 unique differential splicing (DS) events within 4,222 genes (SE = 6,185; A5SS = 410, A3SS = 506, and RI = 526; (**Table S6B-F**), including 233 oncogenes or TSGs (**Figure 5B**). There were 120 genes (2.2%) which were both DE and DS (**Figure 5C, Table S6G**), indicating these may impact total protein

abundance in tumors. DS genes were significantly over-represented for mitotic spindle, E2F targets, G2M checkpoint, and nucleotide excision repair pathways (Bonf-adj $p < 0.05$, **Figure 5D**). To further investigate the impact on DNA repair and other pathways, we performed GSVA of DNA repair and cancer signaling pathways on these DS oncogenes and TSGs and found that depletion of CLK1 leads to upregulation of TNFA, PI3K/AKT/MTOR, IL6/JAK/STAT3, and apoptosis pathway expression and downregulation of multiple DNA repair pathways (**Figures 5E-F and S5C-D**). Importantly, *CLK1* morpholino-mediated knockdown resulted in significant reduction of *CLK1* and additional known targets, *LRP5, AXIN2,* and *LEF1* ($Log_2FC < -0.1$, B-H p-adj < 0.05, **Table S6H**) and downregulation of WNT signaling (**Figure 5E-F**), consistent with a known mechanism of Cirtuvivant[32].

Finally, we asked whether *CLK1 exon 4* inclusion levels affect any of the essential oncogenes defined by the pediatric gene dependency maps of the Childhood Cancer Model Atlas[36]. We observed 18 of these genes also exhibit significant gene dependencies in established pediatric HGG cell lines (**Figure 5F-G, Table S6I, Figure S6**), including seven direct regulators of MAPK signaling: *BRAF, EZH2, RAF1, JUN, FGFR1, FGFR2,* and *SRC*. For instance, the expression levels of mRNAs encoding proto-oncogene *SRC*[37,38] are higher in cells with high *CLK1* exon 4 (non-targeting morpholino), indicating that *CLK1* may enhance or promote *SRC* expression. The differential splicing cases are more complex as they affect multiple transcripts within a gene, but taken together, these data suggest that transcript-level changes mediated through *CLK1* differential exon 4 splicing may contribute to some of these dependencies, particularly DNA repair and MAPK signaling, consistent with the established link between aberrant splicing with cancer progression[39–41].

Discussion

Pediatric brain cancer remains the leading cause of disease-related mortality in children, and HGGs present challenges of chemotherapy resistance and surgical limitations. In this study,

we conducted a large-scale analysis of differential alternative splicing across pediatric CNS tumors, revealing pervasive splicing dysregulation. We introduce the SBI as a quantitative, sample-level metric to measure differential splicing, enabling cross-histology comparisons without the requirement for matched normal controls. Notably, we did not observe our hypothesized inverse relationship between TMB and SBI; instead, we observed a weak but significant positive correlation between TMB and SBI. This suggests that splicing dysregulation in pediatric brain tumors may not simply serve as a compensatory mechanism in genetically "quiet" tumors, but could reflect broader disruptions in RNA processing programs.

Clustering tumors by highly variable skipped exon (SE) events identified 11 splicing-defined groups, many significantly enriched for specific histologies or molecular subtypes. Importantly, Cluster 6 emerged as the poorest prognosis group, enriched for HGGs and characterized by both high splicing variability and upregulation of the spliceosome pathway. This subgroup exhibited the greatest variance in SBI and survival analyses indicated that, paradoxically, higher spliceosome activity was associated with improved outcomes in these otherwise aggressive tumors. This suggests that the functional impact of splicing dysregulation may differ depending on the balance between oncogenic and potentially tumor-suppressive splicing programs.

By integrating RNA-seq–derived exon-level splicing quantification with CRISPR perturbation data and in contrast to GSVA scores, higher exon 4 PSI in *CDC-like kinase 1 (CLK1)*, a critical splicing factor and cell-cycle modulator, was linked to significantly worse prognosis, suggesting that global spliceosome activity and *CLK1*-driven exon inclusion may reflect distinct and potentially opposing aspects of splicing biology in Cluster 6 tumors. This divergence underscores that not all splicing pathway activation is equivalent. Broadly elevated spliceosome activity might reflect a compensatory or less oncogenic program, whereas *CLK1* exon 4 inclusion could mark a more malignant, dependency-associated splicing state.

Experimental modulation of *CLK1*, either through pharmacological inhibition or morpholino-directed exon 4 depletion in the KNS-42 cell line, resulted in significantly reduced cell proliferation and/or viability. Splicing modulation to deplete exon 4 ablated *CLK1* RNA and protein levels. Transcriptomic profiling following *CLK1* exon 4 depletion revealed widespread alterations in the splicing and expression of cancer-relevant genes, with enrichment for cell cycle, DNA repair, and MAPK signaling pathways, many of which are essential dependencies in pediatric HGG cell lines. These findings support the hypothesis that *CLK1*-mediated splicing sustains multiple oncogenic programs in CNS tumors. Notably, CLK family kinases, including *CLK1*, are already under clinical investigation in multiple adult malignancies through early phase trials. The Pan-Clk/Dyrk Inhibitor cirtuvivint (SM08502) is being used in a phase 1 clinical trial in patients with acute myeloid leukemia (AML) and myelodysplastic syndromes (MDS)[42], and has shown preclinical efficacy in non-CNS solid tumors such as castrate-resistant prostate cancer, colorectal cancer, endometrial cancer, and non-small cell lung cancer[32,43–46]. An ATP-competitive, macrocyclic inhibitor of the CLK family, BH-30236[47], is in a Phase 1/1b clinical trial for patients with AML and MDS[48]. Finally, the CLK1-specific inhibitor, CTX-712, is in Phase 1/2 trial for relapsed or refractory AML and high risk MDS[49], underscoring *CLK1* and its family as a target across diverse tumor histologies. Our study extends the rationale for CLK1 inhibition to pediatric brain tumors, particularly those with high splicing burden and exon 4 inclusion.

In summary, our work maps the splicing landscape in pediatric CNS tumors, defines biologically and clinically relevant splicing subgroups, and establishes *CLK1* exon 4 inclusion as a recurrent, functional, and targetable aberration in aggressive pediatric brain tumors. Our approach to characterizing splicing aberrations and their functional consequences paves the way for future research into mRNA splicing-based mechanisms of tumorigenesis, the identification and development of therapies targeting aberrant splice events, and may even guide splicing-based diagnostics, all of which have the potential to improve the therapeutic

landscape for pediatric brain cancers. Finally, we openly share the splicing data for all pediatric CNS tumors as a resource for the oncology community.

Limitations of the study

In this study, initial splicing quantifications were performed using short-read RNA-Seq technology, which limits the interpretation of the full spectrum of splicing variation, particularly larger multi-exon transcripts or with genes that contain a high number of transcripts. While there are proteomics data for over 200 matched pediatric brain tumors publicly available, we were limited in sample size for DIPG or DMG and other HGGs, so it will be important to validate our findings in larger datasets as they become available. We did not have matched normal RNA for any tumor of origin tissue which precluded us from identifying mutually exclusive events that may also play a role in tumorigenesis. For example, within histologies (eg: LGG), the primary site of the tumor can vary widely depending on diagnosis and it would be ideal to match each tumor to its tissue of origin. Although this is not yet possible with available data, the creation of the upcoming developmental GTEx will be critical in the future. We mitigated these normal tissue limitations by utilizing multiple normal control cohorts as well as the SBI metric. Overall, we employed robust statistical techniques, cross-validated our findings with external datasets, and utilized orthogonal approaches and experimental methods where possible.

Funding

This work was funded in part by the National Institutes of Health (R03OD036498 to JLR), the Chad Tough Foundation, the Children's Hospital of Philadelphia Division of Neurosurgery, the CBTN, and the anonymous private investors to the Children's National Hospital Brain Tumor Institute. This research utilized the Common Fund Data Ecosystem (CFDE) Data Coordinating Center (DCC) data and the Velsera CAVATICA cloud platform provided by the CFDE Cloud Workspace Pilot (1OT2OD030162-01) and the Kids First Data

Research Center Cloud Credit Program (U2C HD109731 – 08S1). Additional support was provided by Cure Search for Children's Cancer Foundation Acceleration Initiative Award (ATT) and Mildred L. Roeckle Endowed Chair in Pathology at Children's Hospital of Philadelphia (ATT).

Acknowledgements

We graciously thank all of the patients and families of the Children's Brain Tumor Network (CBTN) and the Pacific Pediatric Neuro-oncology Consortium for donating tissue which enabled this research. The authors thank the following collaborators who contributed experiments, analyses, code, and/or code review that were ultimately not included in the manuscript: Poonam Sonawane, Cullen Wilson, Krutika S. Gaonkar, and Run Jin.

Ethics statement

This study utilized publicly available genomic data from the Open Pediatric Cancer (OpenPedCan) project, derived from the Children's Brain Tumor Network (CBTN) and the Pacific Pediatric Neuro-Oncology Consortium (PNOC). These consortia have established protocols for the ethical collection and sharing of patient data. The patient-derived cell lines 7316-1763 and 7316-1769 were obtained via request from the CBTN, and the KNS-42 cell line was purchased commercially. While this study did not directly involve the collection of new human or animal subject data, the use of these pre-existing resources implies that the original data collection was conducted with appropriate institutional review board approval and informed consent procedures.

Conflicts of Interest

The authors declare no conflicts of interest.

Author Contributions

Conceptualization: ASN, JLR, ACR, RJC, PJS

Methodology: ASN, JLR, RJC, ACR, KSR, AK, SA, KLC, PJS

Software: BE, ASN, RJC, PJS, JLR

Validation: PS, KC, RJC, KLC, KEH, ASN, AL, PS, PJS

Formal Analysis: ASN, JLR, RJC, KLC, KSR, BE, PJS, AS

Investigation: ASN, JLR, RJC, KSR, AK, PJS

Resources: JLR, ACR, ATT, PBS, CB, SJD, Kal LC, DH

Data Curation: JLR, ASN, RJC

Writing - Original Draft: ASN, JLR, KSR, PS, KLC, PJS

Writing - Review & Editing: ASN, JLR, RJC, SJD, KLC, JBF, JMD, PJS

Visualization: ASN, JLR, KSR, RJC, KLC, PJS

Supervision: JLR, ACR, ATT

Project Administration: JLR, ACR

Funding Acquisition: JLR, ACR, PBS, ATT, SJD

Data Availability

Patient genomic data

All pediatric brain tumor raw data are available upon request from the database of Genotypes and Phenotypes (dbGAP), accession number phs002517.v2.p2, and/or from the Children's Brain Tumor Network (https://cbtn.org) and the Pacific Pediatric Neuro-Oncology Consortium (pnoc.us) for data not immediately available in dbGaP. All processed data used in this study were derived from the OpenPedCan project[15] v13 data release at https://github.com/d3b-center/OpenPedCan-analysis. All code for the manuscript analyses and figures are openly available at https://github.com/rokitalab/clk1-splicing.

Non-tumor control RNA-Seq

RNA-Seq data from the GTEx project (dbGAP Accession phs000424) and the Evo-Devo atlas (Array Express Accession E-MTAB-6814) were harmonized with GENCODE v39 using the Kids First Data Resource Center workflow at https://github.com/kids-first/kf-rnaseq-workflow. For this study, we restricted to samples from individuals under 40 years of age.

CLK1 morpholino RNA-Seq

RNA-sequencing data from the *CLK1* morpholino experiment has been deposited in GSE273841.

Merged primary and summary data

Merged primary matrices and summary files utilized in this manuscript were derived from are openly accessible via the download script in the https://github.com/rokitalab/clk1-splicing repository.

References

1. Thorbinson C, Kilday JP. Childhood Malignant Brain Tumors: Balancing the Bench and Bedside. *Cancers* . 2021;13(23). doi:10.3390/cancers13236099

2. Bavle A, Chintagumpala M. Pediatric high-grade glioma: a review of biology, prognosis, and treatment. *J Radiat Oncol*. 2018;7(1):7-15.

3. Baugh JN, Veldhuijzen van Zanten S, Fiocco M, et al. Treatment-related survival patterns in diffuse intrinsic pontine glioma using a historical cohort: A report from the European Society for Pediatric Oncology DIPG/DMG Registry. *Neurooncol Adv*. 2024;6(1):vdae155.

4. Hatoum R, Chen JS, Lavergne P, et al. Extent of Tumor Resection and Survival in Pediatric Patients With High-Grade Gliomas: A Systematic Review and Meta-analysis. *JAMA Netw Open*. 2022;5(8):e2226551.

5. Wu G, Diaz AK, Paugh BS, et al. The genomic landscape of diffuse intrinsic pontine glioma and pediatric non-brainstem high-grade glioma. *Nat Genet*. 2014;46(5):444-450.

6. Mackay A, Burford A, Carvalho D, et al. Integrated Molecular Meta-Analysis of 1,000 Pediatric High-Grade and Diffuse Intrinsic Pontine Glioma. *Cancer Cell*. 2017;32(4):520-537.e5.

7. Siddaway R, Milos S, Vadivel AKA, et al. Splicing is an alternate oncogenic pathway activation mechanism in glioma. *Nat Commun*. 2022;13(1):588.

8. Sehgal P, Naqvi AS, Higgins M, et al. NRCAM variant defined by microexon skipping is a targetable cell surface proteoform in high-grade gliomas. *Cell Rep*. 2025;44(8):116099.

9. Baralle FE, Giudice J. Alternative splicing as a regulator of development and tissue identity. *Nat Rev Mol Cell Biol*. 2017;18(7):437-451.

10. Ule J, Blencowe BJ. Alternative Splicing Regulatory Networks: Functions, Mechanisms, and Evolution. *Mol Cell*. 2019;76(2):329-345.

11. Scotti MM, Swanson MS. RNA mis-splicing in disease. *Nat Rev Genet*. 2016;17(1):19-32.

12. Merkin J, Russell C, Chen P, Burge CB. Evolutionary Dynamics of Gene and Isoform Regulation in Mammalian Tissues. *Science*. 2012;338(6114):1593-1599.

13. Chen S, Yang C, Wang ZW, et al. CLK1/SRSF5 pathway induces aberrant exon skipping of METTL14 and Cyclin L2 and promotes growth and metastasis of pancreatic cancer. *J Hematol Oncol*. 2021;14(1):60.

14. Fuentes-Fayos AC, Vázquez-Borrego MC, Jiménez-Vacas JM, et al. Splicing machinery dysregulation drives glioblastoma development/aggressiveness: oncogenic role of SRSF3. *Brain*. 2020;143(11):3273-3293.

15. Geng Z, Wafula E, Corbett RJ, et al. The Open Pediatric Cancer Project. *bioRxiv*. Published online July 11, 2024. doi:10.1101/2024.07.09.599086

16. Shapiro JA, Gaonkar KS, Spielman SJ, et al. OpenPBTA: The Open Pediatric Brain Tumor Atlas. *Cell Genomics*. 2023;3(7). doi:10.1016/j.xgen.2023.100340

17. Shen S, Park JW, Lu ZX, et al. rMATS: robust and flexible detection of differential

alternative splicing from replicate RNA-Seq data. *Proc Natl Acad Sci U S A*. 2014;111(51):E5593-E5601.

18. Mehmood A, Laiho A, Venäläinen MS, McGlinchey AJ, Wang N, Elo LL. Systematic evaluation of differential splicing tools for RNA-seq studies. *Brief Bioinform*. 2020;21(6):2052-2065.

19. Dubuc AM, Morrissy AS, Kloosterhof NK, et al. Subgroup-specific alternative splicing in medulloblastoma. *Acta Neuropathol*. 2012;123(4):485-499.

20. Arima Y, Hayashi H, Kamata K, et al. Decreased expression of neurofibromin contributes to epithelial-mesenchymal transition in neurofibromatosis type 1. *Exp Dermatol*. 2010;19(8):e136-e141.

21. Petralia F, Tignor N, Reva B, et al. Integrated Proteogenomic Characterization across Major Histological Types of Pediatric Brain Cancer. *Cell*. 2020;183(7):1962-1985.e31.

22. Karni R, de Stanchina E, Lowe SW, Sinha R, Mu D, Krainer AR. The gene encoding the splicing factor SF2/ASF is a proto-oncogene. *Nat Struct Mol Biol*. 2007;14(3):185-193.

23. Kaida D, Schneider-Poetsch T, Yoshida M. Splicing in oncogenesis and tumor suppression. *Cancer Sci*. 2012;103(9):1611-1616.

24. Golan-Gerstl R, Cohen M, Shilo A, et al. Splicing factor hnRNP A2/B1 regulates tumor suppressor gene splicing and is an oncogenic driver in glioblastoma. *Cancer Res*. 2011;71(13):4464-4472.

25. Sebestyén E, Singh B, Miñana B, et al. Large-scale analysis of genome and transcriptome alterations in multiple tumors unveils novel cancer-relevant splicing networks. doi:10.1101/023010

26. Zhu J, Mayeda A, Krainer AR. Exon identity established through differential antagonism between exonic splicing silencer-bound hnRNP A1 and enhancer-bound SR proteins. *Mol Cell*. 2001;8(6):1351-1361.

27. Ninomiya K, Kataoka N, Hagiwara M. Stress-responsive maturation of Clk1/4 pre-mRNAs promotes phosphorylation of SR splicing factor. *J Cell Biol*. 2011;195(1):27-40.

28. Dominguez D, Tsai YH, Weatheritt R, Wang Y, Blencowe BJ, Wang Z. An extensive program of periodic alternative splicing linked to cell cycle progression. *Elife*. 2016;5. doi:10.7554/eLife.10288

29. Aubol BE, Plocinik RM, Keshwani MM, et al. N-terminus of the protein kinase CLK1 induces SR protein hyperphosphorylation. *Biochem J*. 2014;462(1):143-152.

30. Shkreta L, Delannoy A, Toutant J, Chabot B. Regulatory interplay between SR proteins governs CLK1 kinase splice variants production. *RNA*. 2024;30(12):1596-1607.

31. Cardoso-Moreira M, Halbert J, Valloton D, et al. Gene expression across mammalian organ development. *Nature*. 2019;571(7766):505-509.

32. Bossard C, McMillan EA, Creger E, et al. The Pan-Clk/Dyrk Inhibitor Cirtuvivint (SM08502) Exposes Mechanistic Underpinnings of Alternative Splicing As a Therapeutic Vulnerability

in Heme Malignancies. *Blood*. 2021;138:2950.

33. Hillman RT, Green RE, Brenner SE. An unappreciated role for RNA surveillance. *Genome Biol*. 2004;5(2):R8.

34. Uzor S, Zorzou P, Bowler E, Porazinski S, Wilson I, Ladomery M. Autoregulation of the human splice factor kinase CLK1 through exon skipping and intron retention. *Gene*. 2018;670:46-54.

35. Duncan PI, Stojdl DF, Marius RM, Bell JC. In vivo regulation of alternative pre-mRNA splicing by the Clk1 protein kinase. *Mol Cell Biol*. 1997;17(10):5996-6001.

36. Sun CX, Daniel P, Bradshaw G, et al. Generation and multi-dimensional profiling of a childhood cancer cell line atlas defines new therapeutic opportunities. *Cancer Cell*. 2023;41(4):660-677.e7.

37. Dehm SM, Bonham K. SRC gene expression in human cancer: the role of transcriptional activation. *Biochem Cell Biol*. 2004;82(2):263-274.

38. Georgescu MM, Islam MZ, Li Y, et al. Global activation of oncogenic pathways underlies therapy resistance in diffuse midline glioma. *Acta Neuropathol Commun*. 2020;8(1):111.

39. Zhang J, Manley JL. Misregulation of pre-mRNA alternative splicing in cancer. *Cancer Discov*. 2013;3(11):1228-1237.

40. Nomura S, Yoshitomi H, Takano S, et al. FGF10/FGFR2 signal induces cell migration and invasion in pancreatic cancer. *Br J Cancer*. 2008;99(2):305-313.

41. Lawrence MS, Stojanov P, Mermel CH, et al. Discovery and saturation analysis of cancer genes across 21 tumour types. *Nature*. 2014;505(7484):495-501.

42. National Cancer Institute (.gov). June 23, 2016. Accessed December 3, 2024. https://www.cancer.gov/research/participate/clinical-trials-search/v?id=NCI-2024-05326&loc=0&q=SM08502&rl=1

43. Tolcher A, Babiker HM, Chung V, et al. Abstract CT112: Initial results from a Phase 1 trial of a first-in-class pan-CDC-like kinase inhibitor (SM08502) with proof of mechanism in subjects with advanced solid tumors. *Cancer Res*. 2021;81(13_Supplement):CT112-CT112.

44. ClinicalTrials.Gov. Accessed July 25, 2024. https://www.clinicaltrials.gov/study/NCT05084859

45. A. Scott, J. Call, S. Chandana, E. Borazanci, G. Falchook, R. Bordoni, S. Richey, A. Starodub, V. Chung, N. Lakhani, E. Lam, K. Schaffer, J. Wang, G. Shapiro, J. Sachdev, D. Beaupre and A. Tolcher. Preliminary Evidence of Clinical Activity from Phase 1 and 1b Trials of the CLK/DYRK Inhibitor Cirtuvivint (CIRT) in Subjects with Advanced Solid Tumors. Presented at: ESMO; 2022; Paris. https://www.biosplice.com/medium/image/preliminary-evidence-of-clinical-activity-from-phase-1-and-1b-trials-of-cirtuvivint-09092022_922/view.aspx

46. Corr BR, Moroney MR, Woodruff E, et al. Combination CDC-like kinase inhibition (CLK)/Dual-specificity tyrosine-regulated kinase (DYRK) and taxane therapy in CTNNB1-

mutated endometrial cancer. *bioRxivorg*. Published online April 6, 2023. doi:10.1101/2023.04.04.535570

47. Cui JJ, Jiang P, Deng W, et al. Abstract 5944: Discovery of BH-30236: A novel macrocyclic CLK inhibitor targeting alternative splicing in cancers. *Cancer Res*. 2024;84(6_Supplement):5944-5944.

48. National Cancer Institute (.gov). June 23, 2016. Accessed December 3, 2024. https://www.cancer.gov/research/participate/clinical-trials-search/v?id=NCI-2024-06415&loc=0&q=clk&rl=1

49. National Cancer Institute (.gov). June 23, 2016. Accessed December 3, 2024. https://www.cancer.gov/research/participate/clinical-trials-search/v?id=NCI-2023-02412&r=1

Figure Legends

Figure 1: Pediatric brain tumors display heterogeneous global patterns of aberrant splicing.

(A) Circos plot of CNS tumors used in this study, categorized by histology, tumor location, and reported gender. Non-neoplastic tumors consist of benign tumors and/or cysts. **(B)** Lollipop plot illustrating the total number of recurrent differential splicing events across the cohort, classified by splicing type (SE: single exon, RI: retained intron, A3SS: alternative 3' splice site, A5SS: alternative 5' splice site). **(C)** UpsetR plot of recurrent differential SE splicing events (N ≥ 2 of samples within a histology). **(D)** Barplots of the number of histology-specific recurrent SE events per patient. Histologies are reverse-ordered by the total number of unique events (skipping + inclusion). **(E)** Distribution plots of SE splicing burden index (SBI) by histology. Shaded regions represent high (blue; ≥ Quartile 3) and low (yellow; ≤ Quartile 1) SE SBI groups.

Figure 2: Splicing-based clustering reveals heterogeneous tumor groups with distinct histologies, pathway activities, and clinical outcomes.

(A) Hierarchical clustering heatmap of PSI values for top 5,000 most variable SE splice events across tumors. **(B)** Kaplan-Meier curve of EFS for patients by cluster membership. **(C)** Stacked barplot showing histology sample membership fraction for each cluster. **(D)** Heatmap of top cancer-related pathways by cluster (GSVA scores represented by blue/orange color). **(E)** Heatmap of protein abundance for top 30 most variable proteins within the KEGG spliceosome pathway (GSVA scores denote KEGG spliceosome scores) **(F)** Forest plot of cox proportional hazards multivariate interaction EFS model for cluster and KEGG spliceosome GSVA score, including covariates for tumor resection and age at diagnosis. Black and white diamonds indicate statistically significant and not significant hazard ratios (HRs), respectively, with intervals denoting 95% confidence intervals. Gray diamonds indicate reference levels of factor covariates.

Figure 3: Functional splice event prioritization in Cluster 6 nominates *CLK1* Exon 4 inclusion as an oncogenic dependency.

(A) Cox proportional hazards model forest plot of OS among patients in Cluster 6, including covariates for extent of tumor resection, histology group, SE SBI, and age at diagnosis. Black and white diamonds indicate statistically significant and not significant hazard ratios, respectively, with intervals denoting 95% confidence intervals. Gray diamonds indicate reference levels of factor covariates. **(B)** Volcano plot illustrating differentially-expressed splicing factor genes in Cluster 6 tumors with high SBI compared to those with low SBI (NS = not significant, FC = fold change, colored dots represent $\log_2 FC > |.5|$ and/or Benjamini and Hochberg (B-H) adjusted p-value < 0.05). **(C)** Workflow to prioritize candidate differential exon-level splicing events that alter UniProt-defined functional sites in Cluster 6 tumors. Stacked bar plots represent the fraction of exon inclusion, skipping, or mixed splicing events categorized by predicted impact. **(D)** Sashimi plot of two representative tumor samples with either high (BS_30VC3R2Q) or low (BS_FYP2B298) *CLK1* exon 4 inclusion. Reads supporting exon 4

skipping are marked with an asterisk (*), and exon 4 is indicated by a hash (#) on the transcript plot. **(E)** Scatter plot showing log_2-single exon SBI versus log_2-*CLK1* TPM and log_2-*CLK1* ENST00000321356 transcript TPM versus log_2-*CLK1* exon 4 PSI in Cluster 6 samples. Pearson's R and p-value are shown. **(F)** Cox proportional hazards model forest plot of OS or **(G)** EFS among patients in Cluster 6, including covariates for extent of tumor resection, histology group, *CLK1* exon 4 PSI, and age at diagnosis. Black and white diamonds indicate statistically significant and not significant hazard ratios, respectively, with intervals denoting 95% confidence intervals. Gray diamonds indicate reference levels of factor covariates. **(H)** Distribution of *CLK1* exon 4 PSI across age categories in Cluster 6 samples, Evo-Devo tissues, and GTEx controls. All boxplots represent the 25th and 75th percentile and the bar represents the median.

Figure 4. *CLK1* exon 4 is required for pediatric brain tumor cell line growth and viability.

(A) Boxplot of DepMap dependency scores stratified by high or low *CLK1* exon 4 containing transcript expression in brain tumor cell lines. Wilcoxon p-value shown. **(B)** Ranked dotplot of DepMap dependency scores in brain tumor cell lines with pediatric line KNS-42 highlighted in red. **(C)** Proliferation of KNS-42 cells treated with increasing concentrations of pan-DYRK/CLK1 inhibitor Cirtuvivint over six days. **(D)** Day 3 cell viability of KNS-42 cells treated with increasing concentrations of Cirtuvivint. Stars denote Bonferroni-adjusted p-values following pairwise Student's *t-tests*. **(E)** Barplot showing the RNA expression fold-change in cells treated with control morpholino or morpholino targeting the *CLK1* exon 3-4 junction or exon 3-5 junction. **(F)** Western blot of CLK1 with increasing morpholino treatment of 1, 5, and 10 μM. **(G)** Cell viability of cells treated with *CLK1* exon 4 morpholino or non-targeting morpholino. Stars denote within-time paired Student's *t-tests*.

Figure 5. Perturbing *CLK1* disrupts RNA splicing and impairs oncogenic transcriptional programs.

(A) Volcano plot illustrating genes differentially-expressed in KNS-42 cells treated with *CLK1* exon 4 targeting morpholino compared to cells treated with non-targeting morpholino. **(B)** Barplots displaying number of differentially expressed (DE) genes or differentially spliced (DS) genes affecting functional sites categorized by gene family. **(C)** Venn diagram depicting overlap of all DS and DE genes **(D)** Over-representation analysis of HALLMARK and KEGG pathways for DS cancer genes **(E)** Heatmap displaying single-sample HALLMARK GSVA scores for DS genes affecting functional sites in cells treated with *CLK1* exon 4 morpholino or non-targeting morpholino. **(F)** Barplots illustrating the mean GSVA score difference by treatment (n = 3 replicates per treatment). **(G)** Venn diagram depicting overlap of DS and DE genes and significant (Wald FDR < 0.05, z-score < -1.5) dependency genes (DG) identified in matched CBTN HGG cell lines through CRISPR dependency experiments from the Childhood Cancer Model Atlas (CCMA v3). **(H)** Ranked dotplot of significant CRISPR gene dependency mean z-scores for pediatric HGG cell lines with *CLK1* expression and splicing-based target genes highlighted in red and blue, respectively.

Figure 1

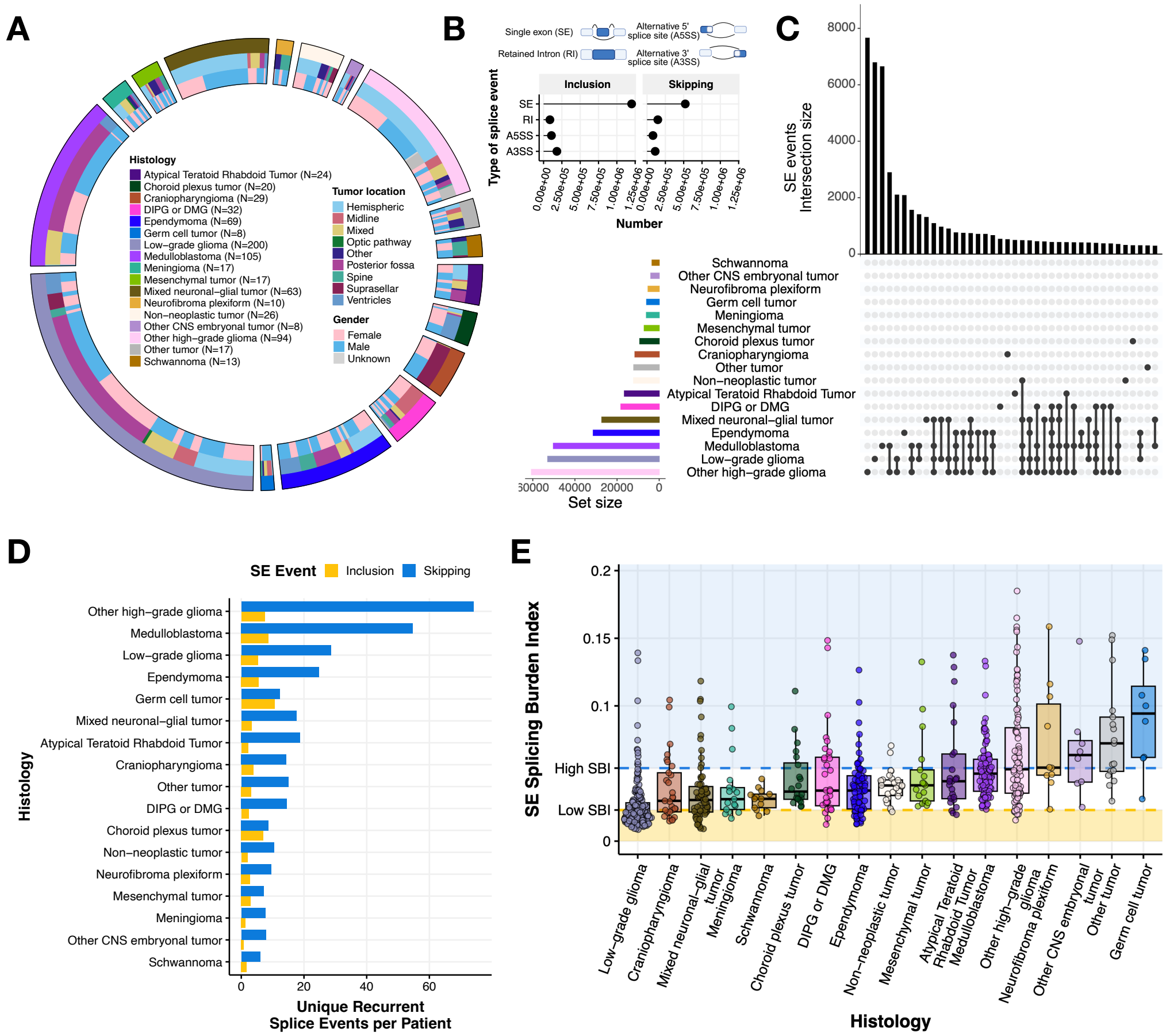
A
Histology
Atypical Teratoid Rhabdoid Tumor (N=24)
Choroid plexus tumor (N=20)
Craniopharyngioma (N=29)
DIPG or DMG (N=32)
Ependymoma (N=69)
Germ cell tumor (N=8)
Low−grade glioma (N=200)
Medulloblastoma (N=105)
Meningioma (N=17)
Mesenchymal tumor (N=17)
Mixed neuronal−glial tumor (N=63)
Neurofibroma plexiform (N=10)
Non−neoplastic tumor (N=26)
Other CNS embryonal tumor (N=8)
Other high−grade glioma (N=94)
Other tumor (N=17)
Schwannoma (N=13)
Tumor location
Hemispheric
Midline
Mixed
Optic pathway
Other
Posterior fossa
Spine
Suprasellar
Ventricles
Gender
Female
Male
Unknown
B
Single exon (SE)
Alternative 5' splice site (A5SS)
Retained Intron (RI)
Alternative 3' splice site (A3SS)
Inclusion
Skipping
Type of splice event
SE
RI
A5SS
A3SS
0.00e+00
2.50e+05
5.00e+05
7.50e+05
1.00e+06
1.25e+06
Number
C
SE events Intersection size
8000
6000
4000
2000
0
Schwannoma
Other CNS embryonal tumor
Neurofibroma plexiform
Germ cell tumor
Meningioma
Mesenchymal tumor
Choroid plexus tumor
Craniopharyngioma
Other tumor
Non−neoplastic tumor
Atypical Teratoid Rhabdoid Tumor
DIPG or DMG
Mixed neuronal−glial tumor
Ependymoma
Medulloblastoma
Low−grade glioma
Other high−grade glioma
60000
40000
20000
0
Set size

D
SE Event
Inclusion
Skipping
Histology
Other high−grade glioma
Medulloblastoma
Low−grade glioma
Ependymoma
Germ cell tumor
Mixed neuronal−glial tumor
Atypical Teratoid Rhabdoid Tumor
Craniopharyngioma
Other tumor
DIPG or DMG
Choroid plexus tumor
Non−neoplastic tumor
Neurofibroma plexiform
Mesenchymal tumor
Meningioma
Other CNS embryonal tumor
Schwannoma
0
20
40
60
Unique Recurrent Splice Events per Patient
E
SE Splicing Burden Index
0.2
0.15
0.1
High SBI
Low SBI
0
Low−grade glioma
Craniopharyngioma
Mixed neuronal−glial tumor
Meningioma
Schwannoma
Choroid plexus tumor
DIPG or DMG
Ependymoma
Non−neoplastic tumor
Mesenchymal tumor
Atypical Teratoid Rhabdoid Tumor
Medulloblastoma
Other high−grade glioma
Neurofibroma plexiform
Other CNS embryonal tumor
Other tumor
Germ cell tumor
Histology

Figure 2

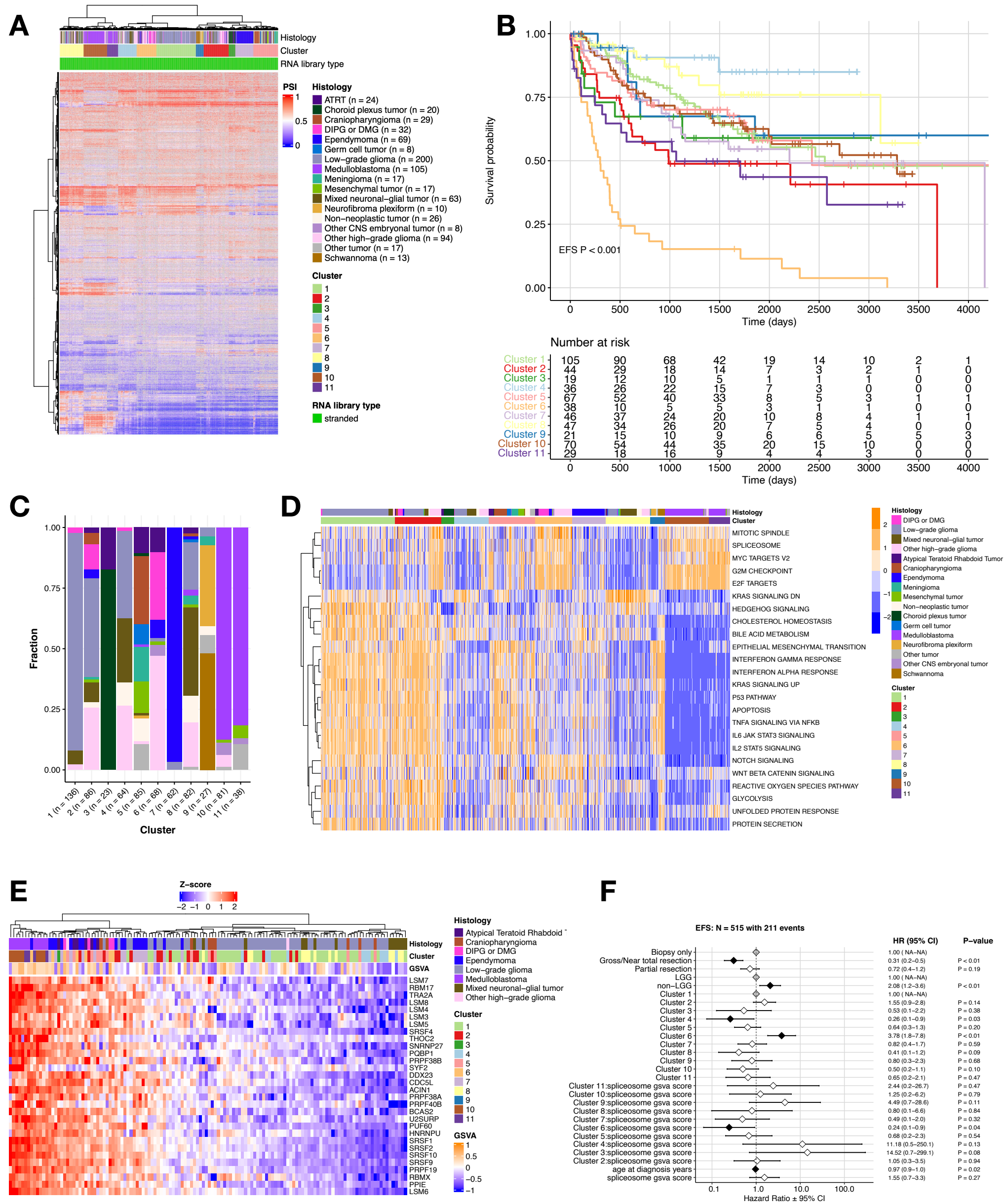
A
Histology
Cluster
RNA library type
PSI
1
0.5
0
Histology
ATRT (n = 24)
Choroid plexus tumor (n = 20)
Craniopharyngioma (n = 29)
DIPG or DMG (n = 32)
Ependymoma (n = 69)
Germ cell tumor (n = 8)
Low−grade glioma (n = 200)
Medulloblastoma (n = 105)
Meningioma (n = 17)
Mesenchymal tumor (n = 17)
Mixed neuronal−glial tumor (n = 63)
Neurofibroma plexiform (n = 10)
Non−neoplastic tumor (n = 26)
Other CNS embryonal tumor (n = 8)
Other high−grade glioma (n = 94)
Other tumor (n = 17)
Schwannoma (n = 13)
Cluster
1
2
3
4
5
6
7
8
9
10
11
RNA library type
stranded
B
Survival probability
1.00
0.75
0.50
0.25
0.00
EFS P < 0.001
0
500
1000
1500
2000
2500
3000
3500
4000
Time (days)
Number at risk
Cluster 1 105 90 68 42 19 14 10 2 1
Cluster 2 44 29 18 14 7 3 2 1 0
Cluster 3 19 12 10 5 1 1 1 0 0
Cluster 4 36 26 22 15 7 3 0 0 0
Cluster 5 67 52 40 33 8 5 3 1 1
Cluster 6 38 10 5 5 3 1 1 0 0
Cluster 7 46 37 24 20 10 8 4 1 1
Cluster 8 47 34 26 20 7 5 4 0 0
Cluster 9 21 15 10 9 6 6 5 5 3
Cluster 10 70 54 44 35 20 15 10 0 0
Cluster 11 29 18 16 9 4 4 3 0 0
C
Fraction
1.00
0.75
0.50
0.25
0.00
1 (n = 136)
2 (n = 86)
3 (n = 23)
4 (n = 64)
5 (n = 85)
6 (n = 68)
7 (n = 62)
8 (n = 82)
9 (n = 27)
10 (n = 81)
11 (n = 38)
Cluster
D
Histology
Cluster
MITOTIC SPINDLE
SPLICEOSOME
MYC TARGETS V2
G2M CHECKPOINT
E2F TARGETS
KRAS SIGNALING DN
HEDGEHOG SIGNALING
CHOLESTEROL HOMEOSTASIS
BILE ACID METABOLISM
EPITHELIAL MESENCHYMAL TRANSITION
INTERFERON GAMMA RESPONSE
INTERFERON ALPHA RESPONSE
KRAS SIGNALING UP
P53 PATHWAY
APOPTOSIS
TNFA SIGNALING VIA NFKB
IL6 JAK STAT3 SIGNALING
IL2 STAT5 SIGNALING
NOTCH SIGNALING
WNT BETA CATENIN SIGNALING
REACTIVE OXYGEN SPECIES PATHWAY
GLYCOLYSIS
UNFOLDED PROTEIN RESPONSE
PROTEIN SECRETION
2
1
0
−1
−2
Histology
DIPG or DMG
Low−grade glioma
Mixed neuronal−glial tumor
Other high−grade glioma
Atypical Teratoid Rhabdoid Tumor
Craniopharyngioma
Ependymoma
Meningioma
Mesenchymal tumor
Non−neoplastic tumor
Choroid plexus tumor
Germ cell tumor
Medulloblastoma
Neurofibroma plexiform
Other tumor
Other CNS embryonal tumor
Schwannoma
Cluster
1
2
3
4
5
6
7
8
9
10
11
E
Z−score
−2 −1 0 1 2
Histology
Cluster
GSVA
LSM7
RBM17
TRA2A
LSM8
LSM4
LSM3
LSM5
SRSF4
THOC2
SNRNP27
PQBP1
PRPF38B
SYF2
DDX23
CDC5L
ACIN1
PRPF38A
PRPF40B
BCAS2
U2SURP
PUF60
HNRNPU
SRSF1
SRSF2
SRSF10
SRSF9
PRPF19
RBMX
PPIE
LSM6
Histology
Atypical Teratoid Rhabdoid
Craniopharyngioma
DIPG or DMG
Ependymoma
Low−grade glioma
Medulloblastoma
Mixed neuronal−glial tumor
Other high−grade glioma
Cluster
1
2
3
4
5
6
7
8
9
10
11
GSVA
1
0.5
0
−0.5
−1
F
EFS: N = 515 with 211 events
HR (95% CI)
P−value
Biopsy only 1.00 (NA−NA)
Gross/Near total resection 0.31 (0.2−0.5) P < 0.01
Partial resection 0.72 (0.4−1.2) P = 0.19
LGG 1.00 (NA−NA)
non−LGG 2.08 (1.2−3.6) P < 0.01
Cluster 1 1.00 (NA−NA)
Cluster 2 1.55 (0.9−2.8) P = 0.14
Cluster 3 0.53 (0.1−2.2) P = 0.38
Cluster 4 0.26 (0.1−0.9) P = 0.03
Cluster 5 0.64 (0.3−1.3) P = 0.20
Cluster 6 3.78 (1.8−7.8) P < 0.01
Cluster 7 0.82 (0.4−1.7) P = 0.59
Cluster 8 0.41 (0.1−1.2) P = 0.09
Cluster 9 0.80 (0.3−2.3) P = 0.68
Cluster 10 0.50 (0.2−1.1) P = 0.10
Cluster 11 0.65 (0.2−2.1) P = 0.47
Cluster 11:spliceosome gsva score 2.44 (0.2−26.7) P = 0.47
Cluster 10:spliceosome gsva score 1.25 (0.2−6.2) P = 0.79
Cluster 9:spliceosome gsva score 4.49 (0.7−28.6) P = 0.11
Cluster 8:spliceosome gsva score 0.80 (0.1−6.6) P = 0.84
Cluster 7:spliceosome gsva score 0.49 (0.1−2.0) P = 0.32
Cluster 6:spliceosome gsva score 0.24 (0.1−0.9) P = 0.04
Cluster 5:spliceosome gsva score 0.68 (0.2−2.3) P = 0.54
Cluster 4:spliceosome gsva score 11.18 (0.5−250.1) P = 0.13
Cluster 3:spliceosome gsva score 14.52 (0.7−299.1) P = 0.08
Cluster 2:spliceosome gsva score 1.05 (0.3−3.5) P = 0.94
age at diagnosis years 0.97 (0.9−1.0) P = 0.02
spliceosome gsva score 1.55 (0.7−3.3) P = 0.27
0.1
1.0
10.0
100.0
Hazard Ratio ± 95% CI

Figure 3

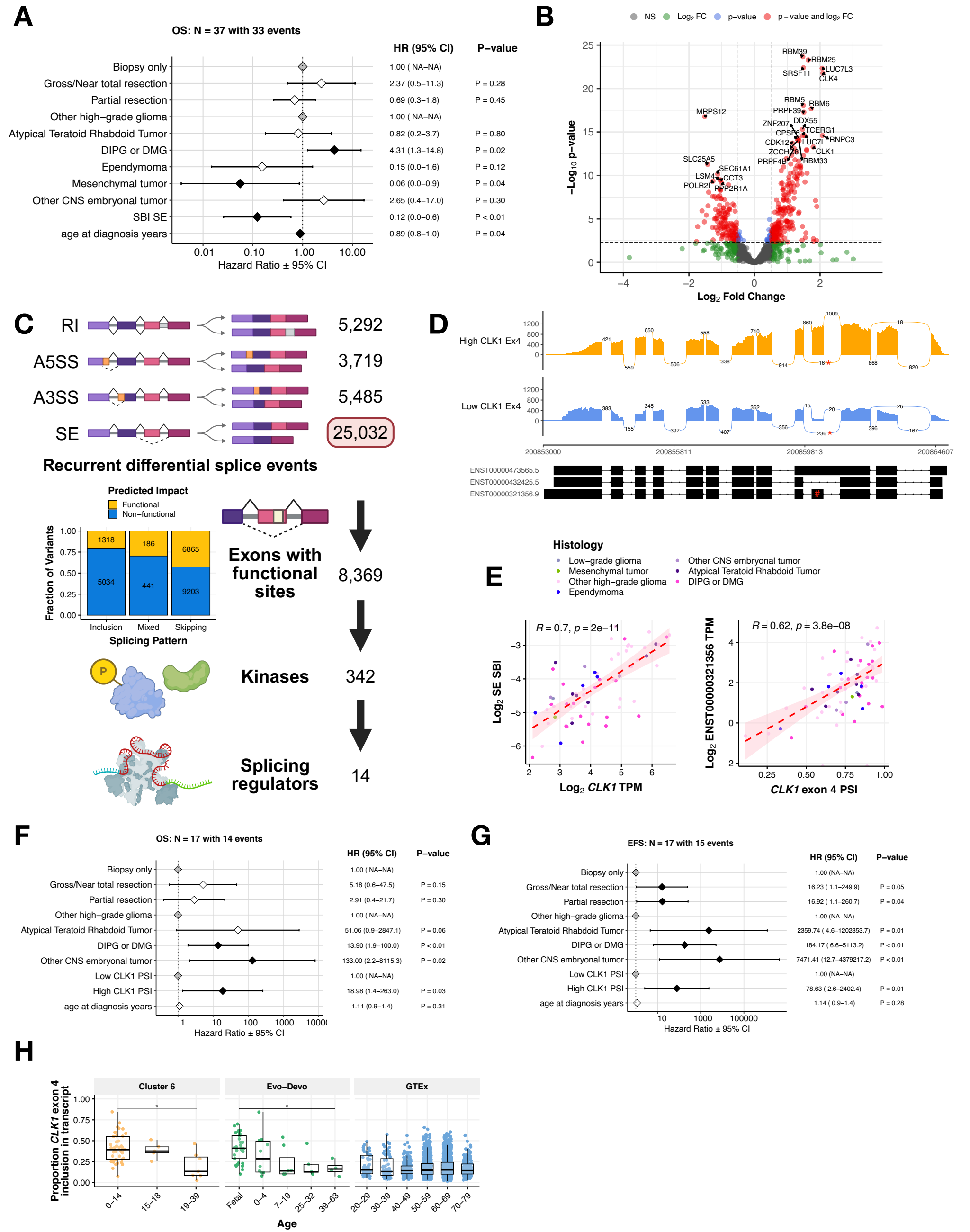
A
OS: N = 37 with 33 events
HR (95% CI)
P–value
Biopsy only 1.00 (NA–NA)
Gross/Near total resection 2.37 (0.5–11.3) P = 0.28
Partial resection 0.69 (0.3–1.8) P = 0.45
Other high–grade glioma 1.00 (NA–NA)
Atypical Teratoid Rhabdoid Tumor 0.82 (0.2–3.7) P = 0.80
DIPG or DMG 4.31 (1.3–14.8) P = 0.02
Ependymoma 0.15 (0.0–1.6) P = 0.12
Mesenchymal tumor 0.06 (0.0–0.9) P = 0.04
Other CNS embryonal tumor 2.65 (0.4–17.0) P = 0.30
SBI SE 0.12 (0.0–0.6) P < 0.01
age at diagnosis years 0.89 (0.8–1.0) P = 0.04
0.01 0.10 1.00 10.00
Hazard Ratio ± 95% CI
B
NS Log2 FC p–value p – value and log2 FC
–Log10 p–value
Log2 Fold Change
RBM39 RBM25 LUC7L3 SRSF11 CLK4 RBM5 RBM6 PRPF39 MRPS12 ZNF207 DDX55 CPSF6 TCERG1 RNPC3 CDK12 LUC7L ZCCHC8 CLK1 PRPF4B RBM33 SLC25A5 SEC61A1 LSM4 CCT3 POLR2I PPP2R1A
C
RI 5,292
A5SS 3,719
A3SS 5,485
SE 25,032
Recurrent differential splice events
Predicted Impact
Functional
Non–functional
Fraction of Variants
1318 186 6865
5034 441 9203
Inclusion Mixed Skipping
Splicing Pattern
Exons with functional sites 8,369
Kinases 342
Splicing regulators 14
D
High CLK1 Ex4
Low CLK1 Ex4
200853000 200855811 200859813 200864607
ENST00000473565.5
ENST00000432425.5
ENST00000321356.9
E
Histology
Low–grade glioma
Mesenchymal tumor
Other high–grade glioma
Ependymoma
Other CNS embryonal tumor
Atypical Teratoid Rhabdoid Tumor
DIPG or DMG
R = 0.7, p = 2e–11
Log2 SE SBI
Log2 CLK1 TPM
R = 0.62, p = 3.8e–08
Log2 ENST00000321356 TPM
CLK1 exon 4 PSI
F
OS: N = 17 with 14 events
HR (95% CI)
P–value
Biopsy only 1.00 (NA–NA)
Gross/Near total resection 5.18 (0.6–47.5) P = 0.15
Partial resection 2.91 (0.4–21.7) P = 0.30
Other high–grade glioma 1.00 (NA–NA)
Atypical Teratoid Rhabdoid Tumor 51.06 (0.9–2847.1) P = 0.06
DIPG or DMG 13.90 (1.9–100.0) P < 0.01
Other CNS embryonal tumor 133.00 (2.2–8115.3) P = 0.02
Low CLK1 PSI 1.00 (NA–NA)
High CLK1 PSI 18.98 (1.4–263.0) P = 0.03
age at diagnosis years 1.11 (0.9–1.4) P = 0.31
Hazard Ratio ± 95% CI
G
EFS: N = 17 with 15 events
HR (95% CI)
P–value
Biopsy only 1.00 (NA–NA)
Gross/Near total resection 16.23 (1.1–249.9) P = 0.05
Partial resection 16.92 (1.1–260.7) P = 0.04
Other high–grade glioma 1.00 (NA–NA)
Atypical Teratoid Rhabdoid Tumor 2359.74 (4.6–1202353.7) P = 0.01
DIPG or DMG 184.17 (6.6–5113.2) P < 0.01
Other CNS embryonal tumor 7471.41 (12.7–4379217.2) P < 0.01
Low CLK1 PSI 1.00 (NA–NA)
High CLK1 PSI 78.63 (2.6–2402.4) P = 0.01
age at diagnosis years 1.14 (0.9–1.4) P = 0.28
Hazard Ratio ± 95% CI
H
Cluster 6
Evo–Devo
GTEx
Proportion CLK1 exon 4 inclusion in transcript
0–14 15–18 19–39 Fetal 0–4 7–19 25–32 39–63 20–29 30–39 40–49 50–59 60–69 70–79
Age

Figure 4

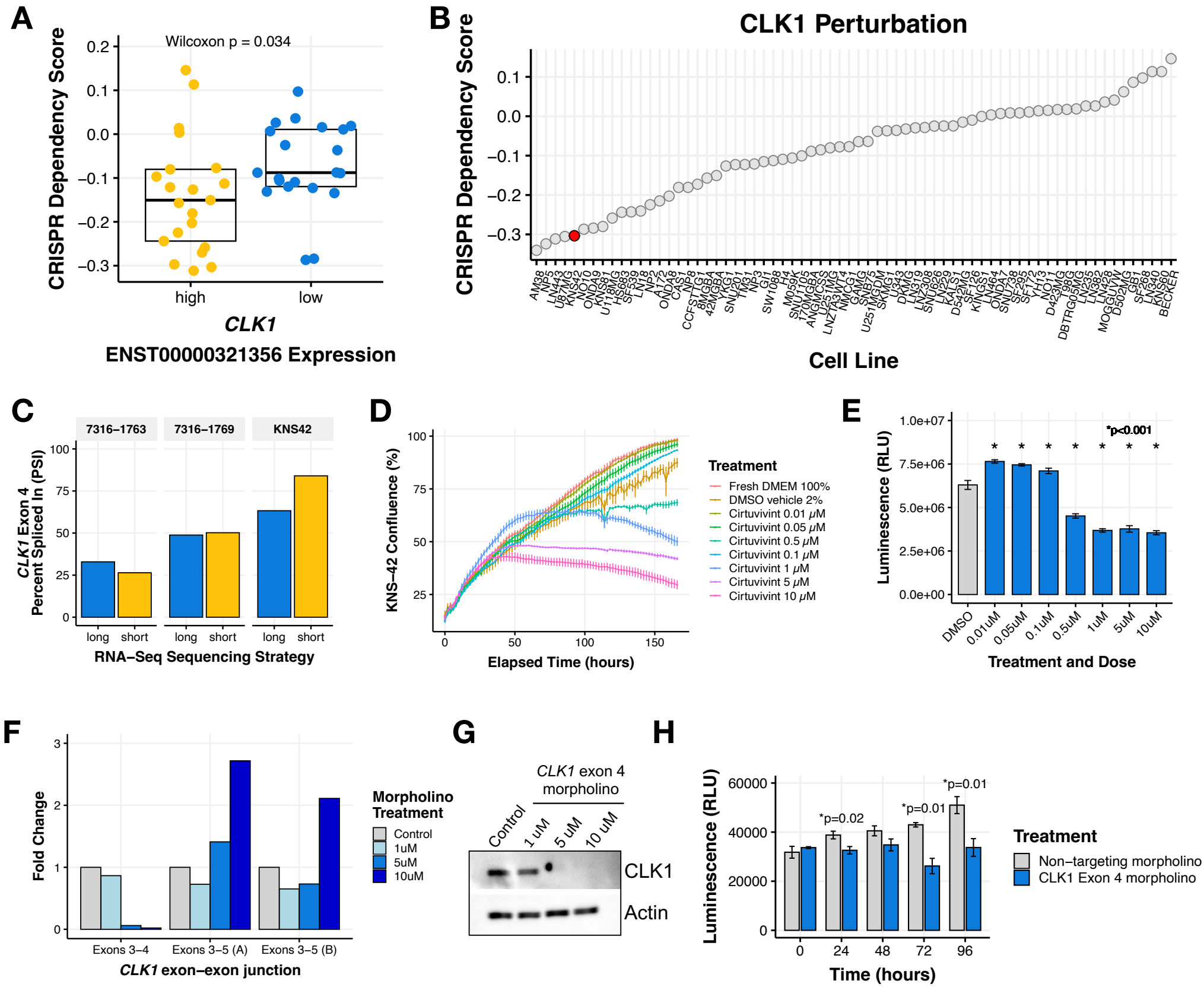
A
Wilcoxon p = 0.034
CRISPR Dependency Score
high
low
CLK1
ENST00000321356 Expression
B
CLK1 Perturbation
CRISPR Dependency Score
Cell Line
C
7316–1763
7316–1769
KNS42
CLK1 Exon 4 Percent Spliced In (PSI)
long
short
RNA–Seq Sequencing Strategy
D
KNS–42 Confluence (%)
Elapsed Time (hours)
Treatment
Fresh DMEM 100%
DMSO vehicle 2%
Cirtuvivint 0.01 μM
Cirtuvivint 0.05 μM
Cirtuvivint 0.5 μM
Cirtuvivint 0.1 μM
Cirtuvivint 1 μM
Cirtuvivint 5 μM
Cirtuvivint 10 μM
E
*p<0.001
Luminescence (RLU)
DMSO
0.01uM
0.05uM
0.1uM
0.5uM
1uM
5uM
10uM
Treatment and Dose
F
Fold Change
Exons 3–4
Exons 3–5 (A)
Exons 3–5 (B)
CLK1 exon–exon junction
Morpholino Treatment
Control
1uM
5uM
10uM
G
CLK1 exon 4 morpholino
Control
1 uM
5 uM
10 uM
CLK1
Actin
H
Luminescence (RLU)
*p=0.02
*p=0.01
*p=0.01
Time (hours)
Treatment
Non–targeting morpholino
CLK1 Exon 4 morpholino

Figure 5

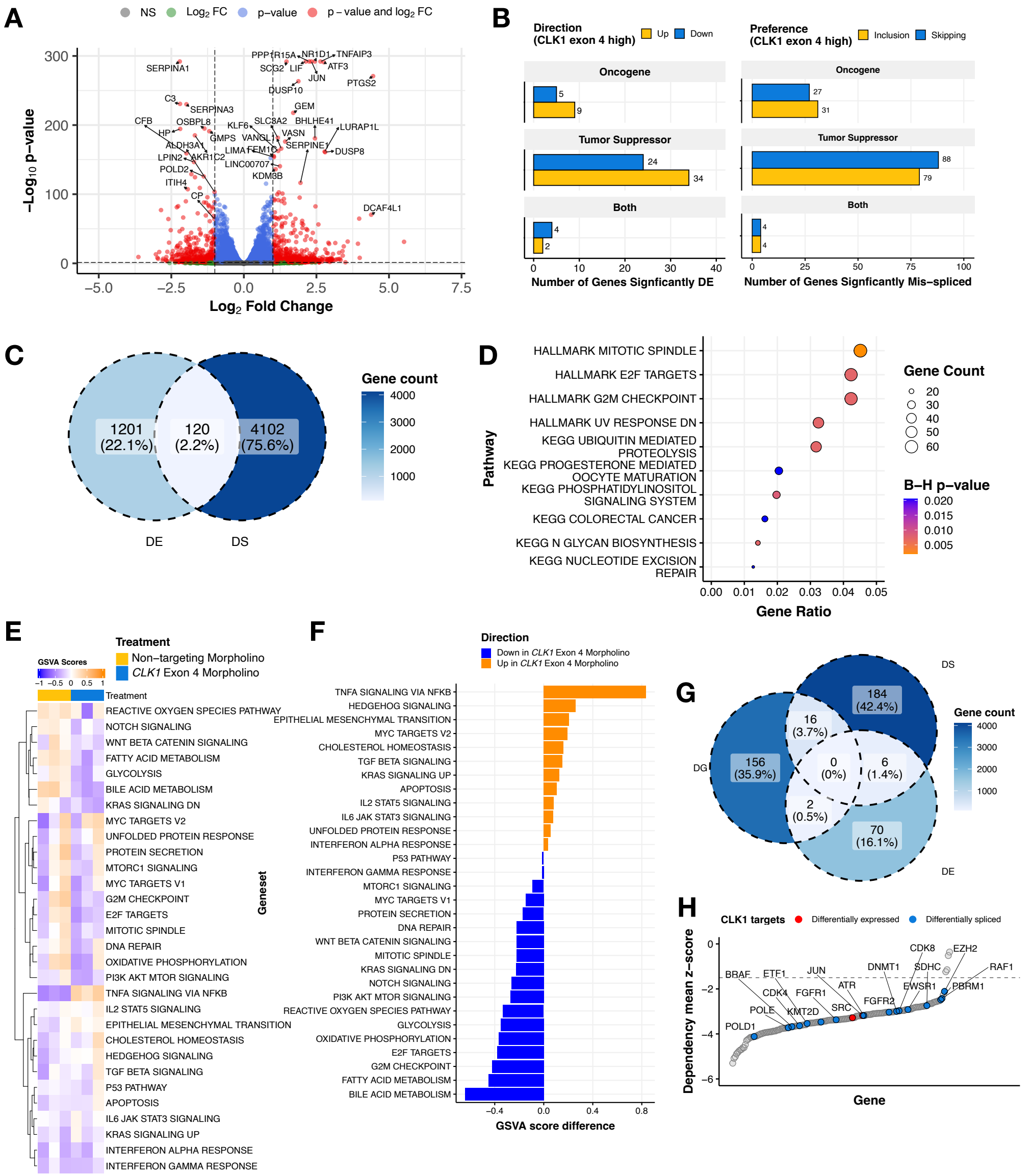
A
NS
Log2 FC
p–value
p – value and log2 FC
–Log10 p–value
Log2 Fold Change
SERPINA1
PPP1R15A
NR1D1
TNFAIP3
SCG2
LIF
ATF3
JUN
PTGS2
DUSP10
C3
SERPINA3
GEM
CFB
OSBPL8
KLF6
SLC3A2
BHLHE41
LURAP1L
HP
GMPS
VANGL1
VASN
ALDH3A1
LIMA1
FEM1C
SERPINE1
DUSP8
LPIN2
AKR1C2
LINC00707
POLD2
KDM3B
ITIH4
CP
DCAF4L1
B
Direction (CLK1 exon 4 high)
Up
Down
Preference (CLK1 exon 4 high)
Inclusion
Skipping
Oncogene
Tumor Suppressor
Both
Number of Genes Signficantly DE
Number of Genes Signficantly Mis–spliced
C
Gene count
1201 (22.1%)
120 (2.2%)
4102 (75.6%)
DE
DS
D
HALLMARK MITOTIC SPINDLE
HALLMARK E2F TARGETS
HALLMARK G2M CHECKPOINT
HALLMARK UV RESPONSE DN
KEGG UBIQUITIN MEDIATED PROTEOLYSIS
KEGG PROGESTERONE MEDIATED OOCYTE MATURATION
KEGG PHOSPHATIDYLINOSITOL SIGNALING SYSTEM
KEGG COLORECTAL CANCER
KEGG N GLYCAN BIOSYNTHESIS
KEGG NUCLEOTIDE EXCISION REPAIR
Pathway
Gene Ratio
Gene Count
B–H p–value
E
GSVA Scores
Treatment
Non–targeting Morpholino
CLK1 Exon 4 Morpholino
Geneset
F
Direction
Down in CLK1 Exon 4 Morpholino
Up in CLK1 Exon 4 Morpholino
GSVA score difference
G
DS
DG
DE
184 (42.4%)
16 (3.7%)
156 (35.9%)
0 (0%)
6 (1.4%)
2 (0.5%)
70 (16.1%)
Gene count
H
CLK1 targets
Differentially expressed
Differentially spliced
Dependency mean z–score
Gene